MULTIFIDELITY COSIMULATION OF HYDROGEN FUEL CELL AERO ENGINE

Vlad Goldenberg
SoftInWay, Inc.

Clement Joly
SoftInWay, Inc

Benjamin Conser
SoftInWay, Inc

Vladyslav Kotechenkov
SoftInWay UK

Viktor Yevlakhov
SoftInWay, Switzerland

Leonid Moroz
SoftInWay, Inc

ABSTRACT

This work demonstrates a complete system simulation of a hydrogen fuel cell electric aero engine that utilizes multifidelity models in an integrated co-simulation. It demonstrates that the inputs to the full simulation model can be configured in the same way as physical control system inputs and physical boundary conditions.

The system architecture consists of a prop-fan powered by an electric motor, which is variable speed. The electrical power to drive the prop-fan comes from a hybrid fuel cell electrical system consisting of a hydrogen fuel cell, turbogenerator, and a supercapacitor battery. The purpose of the battery is short-term power augmentation for takeoff and acceleration, and is envisioned as a lithium-ion supercapacitor, although its exact chemistry is not pertinent to the work and not modelled in focus detail. The fuel cell is aspirated via a two-stage centrifugal compressor drawing air from the front of the engine and driven by a compact electrical motor with a variable speed drive. The compressor discharge air is aftercooled in order to decrease its temperature to near 80 °C, which is the optimum operating temperature of the fuel cell. The exhaust of the fuel cell, which consists of water vapor, nitrogen, and excess air is expanded through an energy recovery turboexpander that is directly coupled on a single shaft with the compressor (combined called the turbocompressor) to reduce the parasitic power demand from the compressor. The fuel cell is cooled with an active cooling system. It is assumed that the hydrogen fuel is pressurized via a tank and controlled via an upstream valving and circulation system.

The following modeling paradigms are used for the subsystem components. The overall system is governed by a lumped-parameter (0D) thermofluid cycle/system model. For most subcomponents, a fidelity enhancement is used. The turbomachinery uses 1D throughflow loss component models that accurately simulate the fluid-dynamic behavior of the turbomachinery flowpaths, as distinct from a limiting but historically-accepted map-based approach. The fuel cell is actively cooled with a liquid cooling system that is modeled using 1D correlations that model the heat transfer (Nusselt correlations) and pressure loss (Moody correlations).

In this work, we develop a full propulsion system model in the commercial simulation code AxSTREAM® System Simulation™. This model is then used to analyze operating conditions

throughout the flight envelope of the engine, which includes takeoff, low altitude flight, high altitude cruise, and high-altitude maximum power. Throughout the analysis, all major subcomponent models (motors, turbocompressor, turboexpander, fuel cell stack, and thermal management subsystem) have realistic analytical models that simulate the performance and operation of each individual component so that appropriate control actuation parameters are used in the model to evaluate the main system controllability and stability. Further, secondary system control actuation parameters pertaining to thermal management and maintenance of the appropriate fuel cell stack environment are evaluated. Therefore, in this work, a complete system model is demonstrated that can be used to design the controls strategy for a complete system, among many other benefits.

The outcome is that the boundary conditions are the physical boundary conditions of flight velocity and altitude. The control inputs are the propfan power input, compressor speed, and fuel cell internal average temperature setpoint. All other system interrelations are inherently modeled via the simulation. Thus, the compressor speed governs the airflow through the fuel cell aspiration and cell pressure through interaction of the pressure drops through the aspirant subsystem and turboexpander backpressure-flow simulation.

NOMENCLATURE, ACRONYMS, ABBREVIATIONS

FADEC	Full Authority Digital Engine Control
PEM	Proton Exchange Membrane
FC	Fuel Cell
F_d	Drag force
C_d	drag coefficient correlated to wing surface area
V_∞	free-stream air velocity or flight speed
Re	Reynolds number
Pr	Prandtl Number
Nu	Nusselt Number
$\dot{Q}$	Heat generation and rejection rate in fuel cell and cooling
λ	Darcy friction factor

INTRODUCTION

The development of revolutionary technologies and aerospace engines involves design uncertainty and risks. Even novel architectures of existing technologies involve similar uncertainties in determination of how a new design that has not been physically built or tested performs at various operating conditions. 3D Multiphysics numerical simulations which are rooted in fundamental physics have advanced to the point where they may be routinely used for digital verification of individual subcomponent design. However, an entire complex system comprised of many interconnecting subsystems and multidisciplinary physics is still too complex to effectively use fully 3D Multiphysics simulation during the system and component development phases because the combined challenges of computational resource demands while

ensuring convergence robustness is extensive. An example of a very recent documented pathway to such Multiphysics and multi-fidelity coupling is documented in (Schuff, 2023)[1].

As alluded to previously, the benefits of developing a simulation model are numerous. For established technology such as turbofan, turbojet, and turboprop engines, for example, simulation models enable risk mitigation when developing new architectures or evaluating novel feature development like alternate secondary flow and turbine cooling schemes, for instance. Thus, the benefits in the development cycle of a new engine are the ability to predict effects at conditions that may be quite disparate from a nominal or rated design point and which may not be immediately obvious to the design engineers working on its development.

For new technologies, such as hydrogen electric fuel cell engine architectures that have the promise of at least partially enabling zero-carbon emission air travel and are the central focus subject of the present work, the impetus to develop holistic simulation models is even greater. Unlike jet engines, nobody has actually operated a real, practical, fuel cell architecture that has the end-use complexity in practice on an aircraft. While fuel cell power systems have been demonstrated on an aircraft by a handful of startup companies in this field, there is really no real-life data to enlighten designers regarding system operation of various architectures under the wide range of operational conditions the systems may encounter. Therefore, robust simulations of these systems that are rooted in physics, empirical data, and understood principles are a key enabler that will answer questions. For example, questions about the difference in system response under altitude/pressure variation when the aspiration compressor is coupled to the main drive shaft versus operating from its own electromotor can be competently answered and used to inform architecture and component design optimization activities.

In addition to usefulness in the development cycle, there is generally a consensus that digital twins of existing systems are useful in evaluating performance and condition monitoring. The fundamental models are developed in the design phase and updated as higher fidelity data becomes available during the lifecycle of the system.

Furthermore, how a complete system behaves under control inputs is a very important design aspect of the control system, since the system being designed must be controllable by the physical actuation methods that are available or designed into the system. This question is investigated for the chosen system. It will be specifically shown that we are able to develop a simulation model that takes into account the most important subcomponent interactions and operate it in simulation in the same way that a control system or operator may operate the real system. In this way, important control laws can be developed for the system that enable it to be controlled by a FADEC or similar subsystems in a way that maximizes efficiency, other performance metrics, and maintains the system within specified operating parameters.

Finally, it must be noted that emphasis is placed in this work on holistic system modeling. This means that the fundamental intercomponent interactions between each other as part of the system are taken into account by designing and implementing subcomponent models of sufficient

[1] (Schuff, 2023)

fidelity to respond to changes in their boundary conditions. As far as the authors are aware, a robust and multifidelity co-simulation model of a fuel cell system has not yet been demonstrated in the literature. Our assertion for what is done should be compared to the typical implementation of aircraft engine models, a fairly recent example of which is presented in (Zaccaria, Stenfelt, Aslanidou, & Kyprianidis, 2018)[2] where the subcomponent fidelity is based on 0D thermodynamic performance metrics. In the present approach, the key turbomachinery components use 1D models that take into account actual designed flow path geometry and operating conditions. Thus, the variation in flow rates, pressure ratios, heat flows, and other system attributes are representative for how the system would behave under the given control inputs, and is therefore a holistic system model.

The rest of this paper is organized in the following way. The forthcoming section will present the fundamental engine model that has been developed and investigated. Then, the turbomachinery component design and resulting baseline performance will be presented. Following this, the fuel cell design and 1D model will be shown and validated. The thermal management system for the fuel cell will then be discussed in detail and it will be shown how it was designed, the method of control, and how it interacts with the greater system. The methodology behind the holistic system simulation model will then be presented after this, and then we will discuss system control aspects from a physical and control perspective. Finally, the simulation results and analysis will be discussed, and several conclusions drawn.

FUNDAMENTAL ENGINE MODEL

The fundamental engine model is a hybrid fuel cell electric power system that may enable carbon-neutral aviation by using hydrogen as the fuel and energy carrier. This system uses high efficiency electrical motors to rotate a fan or propeller that would otherwise be powered by a combustion gas turbine. Electric power comes from a fuel cell consuming hydrogen fuel and oxidized by ambient air. Aspiration of the fuel cell is one of the most critical subsystems, especially for aviation applications where the lower pressure air at higher altitudes requires the aspiration compressor to generate a substantial pressure ratio to deliver sufficient air to the fuel cell to maintain high efficiency and power. The high pressure ratio also introduces parasitic loads from the compressor, which may be quite substantial in comparison to the overall power produced by the fuel cell. To mitigate this, an exhaust turboexpander is used to recover the energy, and a recuperator is used to both recover thermal energy and cool the aspirant air sufficiently to enable reliable fuel cell operation. The fuel cell is a low-temperature PEM type, and can therefore only withstand moderate temperatures, typically not exceeding 80°C - 100°C. The fuel cell uses stored hydrogen as the fuel and compressed ram air as the oxidizer. We assume in the present work that it is desirable to allow the fuel cell to operate at a nominal temperature of 80°C where low-temperature PEM fuel cells operate most effectively. The schematic representation of the power system is shown in Figure 1.

[2] (Zaccaria, Stenfelt, Aslanidou, & Kyprianidis, 2018)

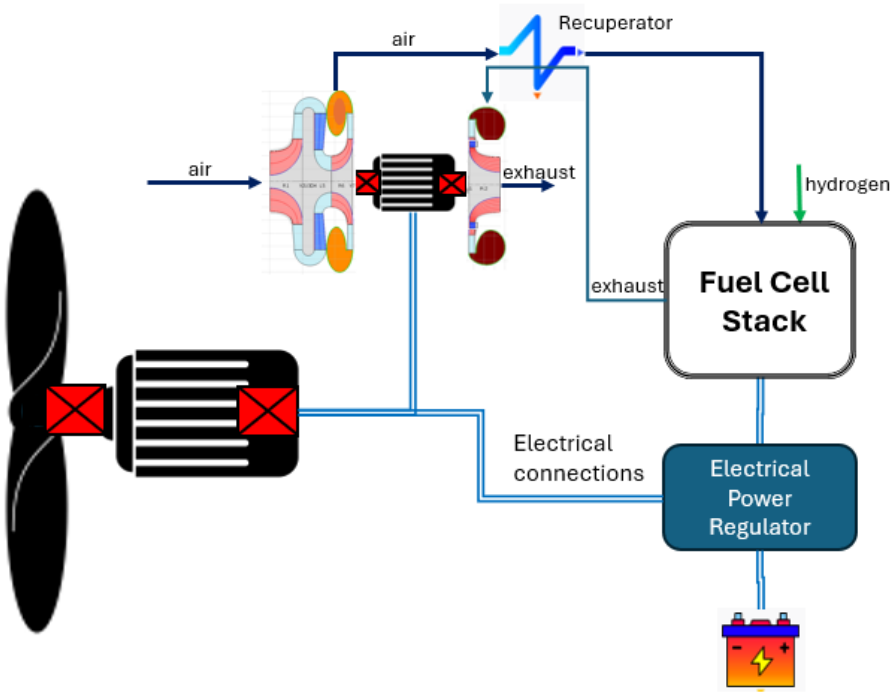

Figure 1 Schematic representation of engine power system. No auxiliary subsystems, most notable the thermal management system, are shown.

The system parameters have been designed so that at nominally full power the fuel cell generates 1MWe, and ultimately the useful power delivered to the drive motor for the propulsion fan is nominally 958kW. This corresponds with, for example, the capabilities of a PT6 engine. Given that the initial implementation of hydrogen electric aero drivetrains will likely be on regional planes in the next decade, a craft such as the Beechcraft 1900, among others, is envisioned here as a typical case.

A 0D model of the propulsion system consisting of ambient conditions, propeller, intake, electro-motor, compressor, turbine, recuperator, cooler, PEM fuel cell, hydrogen supply system (storage, valve and heater) as well as the corresponding electrical components was created in AxSTREAM System Simulation™.

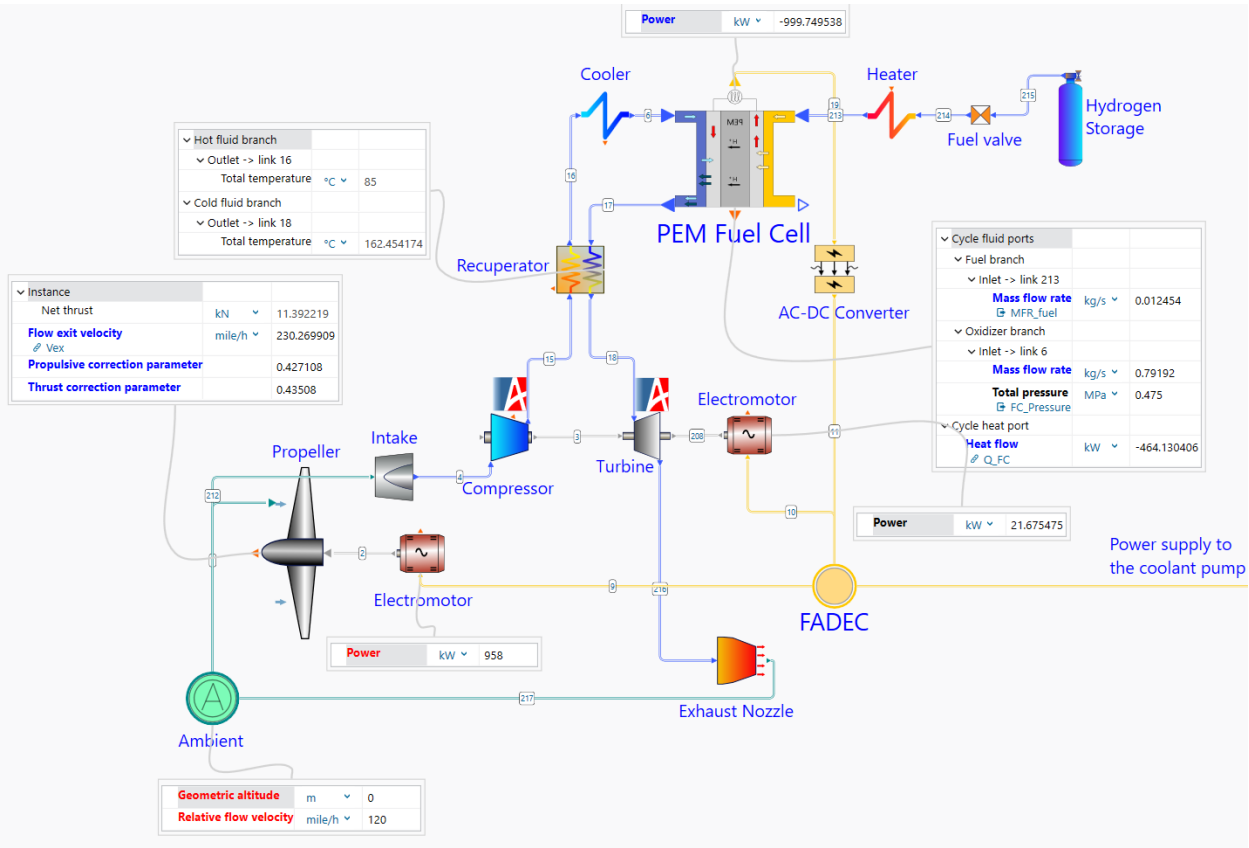

Figure 2 AxSTREAM System Simulation model of the engine with results for take-off conditions

To determine the hybrid system operating conditions, including the design point for the turbomachinery, fuel cell, and thermal management system, thrust calculations at take-off and cruise were performed using the model from Figure 2 so that the overall system may be sized appropriately throughout the various expected flight phases. The take-off and cruise conditions for the engine yield the following results, respectively:

Table 1 Aircraft Engine Performance - Multiple Operating Conditions

	Take Off	**Low Altitude Cruise**	**High Altitude Cruise**
Altitude [m]	0	50	5400
Atmospheric Pressure [kPa]	101.3	100.7	51.23
Atmospheric Temperature [°C]	15	14.7	-20.1
Flight Speed [m/s]	54	103	134
Drag [kN] *reference value only	1.9	6.9	6.9
Engine Power [kW]	958	958	958

Total level flight thrust values (for the airplane, not per engine) were computed for different altitudes (and corresponding ambient air density) and flight speeds using the Beechcraft 1900 wing surface area (28.8 m^2) and an average drag coefficient (C_d) value calculated based on recent airframes (Boeing 737-800 and Airbus A320) – 0.038 – in order to verify the software calculated thrusts. The results are shown in Figure 3. They are derived using Equation 1 from ground level (altitude 0 m) to the expected cruise altitude (5400 m) and beyond, up to the cruise flight speed of the Beechcraft 1900; 134 m/s. It is assumed here that at level flight, the overall airplane drag (Eq. 1) is equal to its thrust, therefore determining our system requirements.

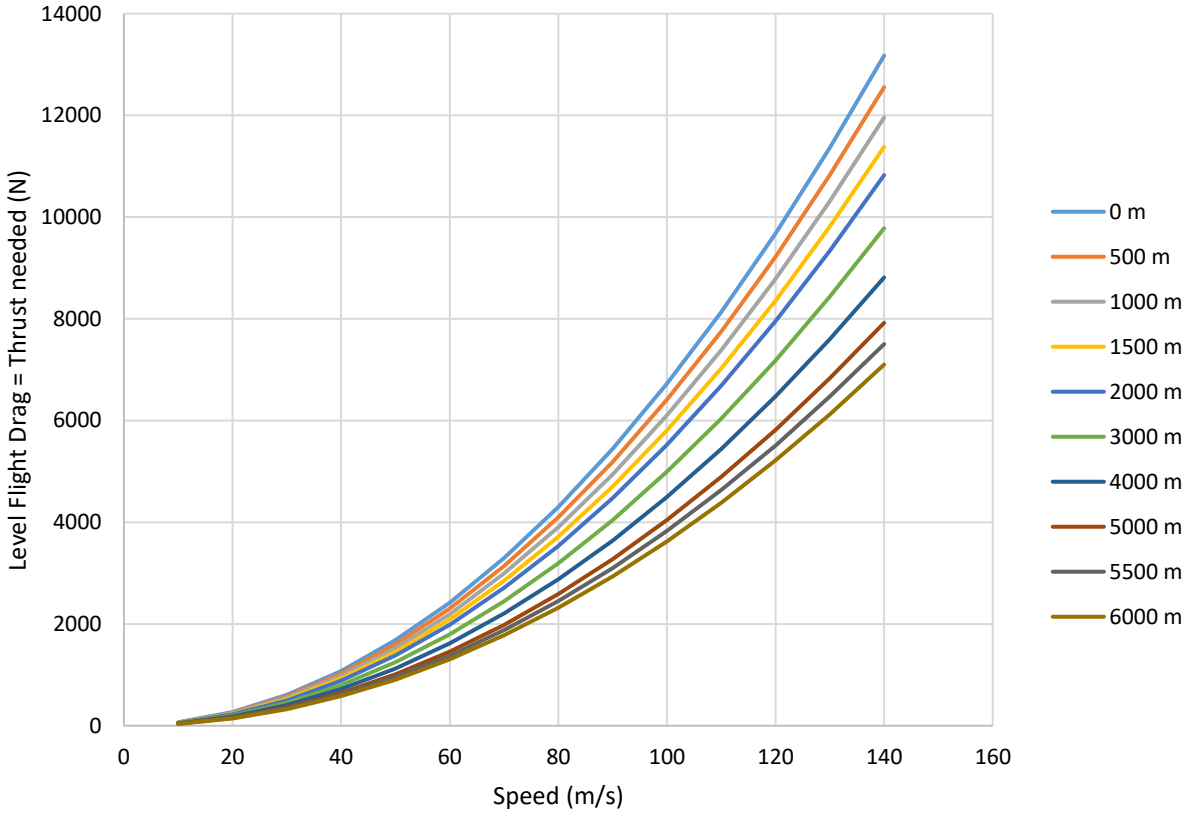

Figure 3 Level fight thrust calculations at different altitudes and flight speeds

$$F_d = \frac{1}{2} C_d A_{wing} \rho_{air} v_\infty^2 \quad (1)$$

Similarly, the ideal power required to drive the propeller can be plotted (Figure 4). To stay agnostic to the propulsor, whether a propfan or ducted fan of any particular design and architecture, the results of Figure 4 are for ideal power and thus assume 100% propulsor efficiency which can be approached but never achieved. A simplified treatment by (Loftin, 1985)[3] shows that propulsive efficiency can be estimated by the formula of Equation 2.

[3] (Loftin, 1985)

$$\eta_p = \frac{2}{2+\frac{\Delta V}{V_\infty}} \quad (2)$$

Where ΔV is the air average velocity gain in the propfan stream and V_∞ is the freestream velocity. If a fairly reasonable assumption is made that at level flight the approximate velocity increases is on the same order of magnitude as the freestream velocity, a propulsor efficiency in the 60%-70% range is estimated. It can therefore be seen from Figure 4 that the desired flight speed of 134 m/s at 5400 m altitude is achievable with the 958 kW electric motor per engine, with about 1200kW total available thrust power for a typical aircraft.

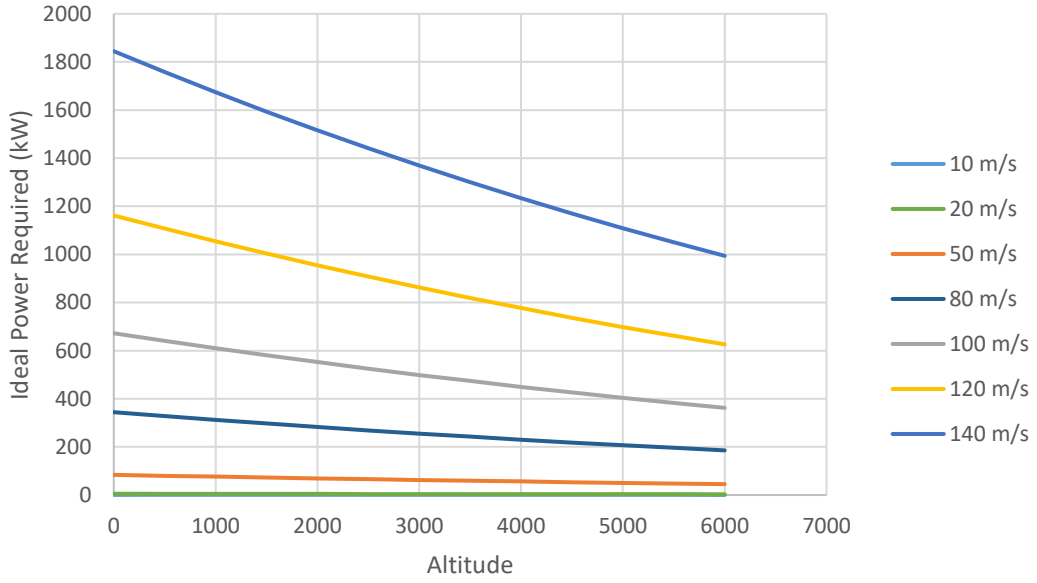

Figure 4 Ideal power required to maintain level flight

TURBOMACHINERY FLOWPATH

Compressor

The compressor is a high-performance centrifugal compressor designed for use in modern aviation propulsion systems. This compressor is a critical component in the proposed hybrid prop-fan engine, which may be utilized in the considered class of aircraft. The compressor's design and operation are optimized for efficiency and operating range under the rigorous conditions encountered in aviation environments.

The compressor flow path design and the performance estimation of the designed flow path were calculated using AxSTREAM® and its respective modules and solvers. Reduced order modeling techniques based on Aungier[4] were used for the 1D performance predictions that were then used

[4] (Aungier, 2000)

as part of the co-simulation model (see Holistic System Simulation Model part on page 25) with the system simulation (presented in Fundamental Engine Model on page 4). When performing the flow path design, a rated condition near cruise altitude was taken as the design point, which therefore implied lower than sea-level pressure and temperature. This choice was made with the recognition that the compressor must be able to supply sufficient airflow to fully oxidize the needed fuel at full power conditions whle supplying sufficient pressure to maintain efficiency. It was recognized that this choice will result in higher than needed air mass flow and pressure near ground conditions, which is easily mitigated by speed reduction.

The compressor is designed for integration with the fuel cell power system that includes a turboexpander and electromotor. Its compact design, with overall length of 111 mm and a diameter of 130 mm (without volute) allows for easy integration and has relatively low mass, which is crucial in aerospace applications. It should be noted that while detailed mechanical design of the compressor is outside the scope of this work, the design takes into consideration good engineering design practices to ensure the machine is overall manufacturable, mechanically and rotordynamically sound, even though detailed mechanical, structural, or rotordynamic analysis was not explicitly performed.

The compressor consists of two centrifugal stages which are aerodynamically profiled to maximize pressure rise per stage while minimizing losses due to shock waves and boundary layer separation. Between impeller stages, the deswirler is present to minimize aerodynamic losses. The compressor is placed on a single shaft with the turbine and electromotor and is supported by FADEC (Full Authority Digital Engine Control). The actions of the FADEC are virtually simulated within the system simulation part of the model (see System Control on page 26).

At the design point, the compressor operates at 56000 RPM and achieves a pressure ratio of 4.1 with and efficiency of 79% at a mass flow of 0.63 kg/s, which is necessary for fuel cell operation and therefore achieving the desired power.

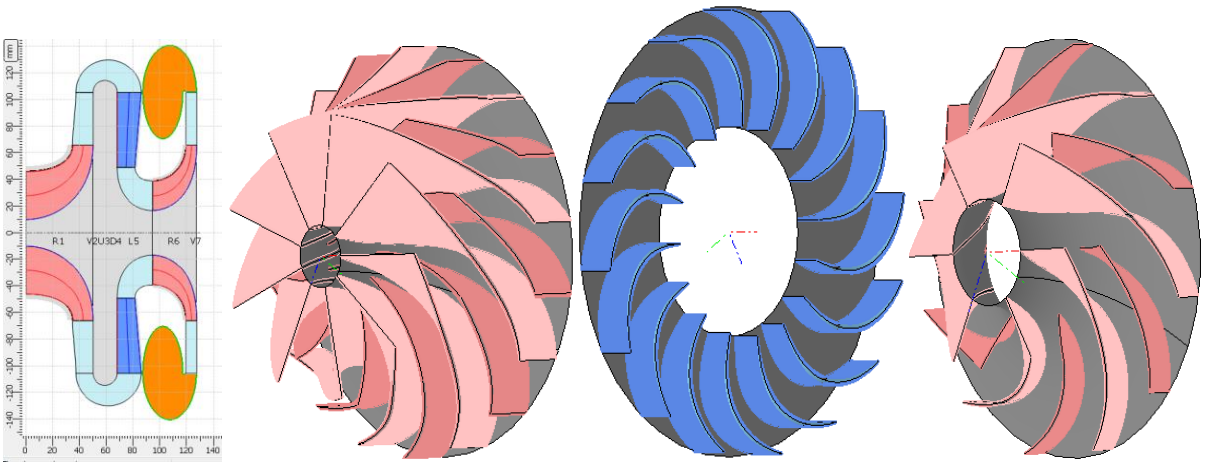

Figure 5: Full compressor meridional section view, first stage impeller, deswirler, and second stage impeller 3D rendering (from left to right)

The compressor is engineered to deliver high efficiency across a wide range of operating conditions, making it suitable for various phases of flight, including takeoff, low-altitude cruise, high-altitude cruise and high-altitude maximum thrust.

In off-design conditions, the compressor maintains robust performance with a pressure ratio variation of ~1.6-6 across the operating envelope. This versatility is critical for maintaining engine performance and fuel cell efficiency under varying altitudes, speeds and power settings.

The performance map of compressor illustrated in Figure 6, provides a detailed view of the relationship between the pressure ratio, mass flow rate and rotational speed. It must be emphasized that the performance map shown is for a set of speedlines ranging from 38,000RPM to 58,000RPM and for illustrative purposes only to show the relative operational range of the design. The map presented is not used in the co-simulation. Rather, the direct calculation model is used for a fully coupled simulation.

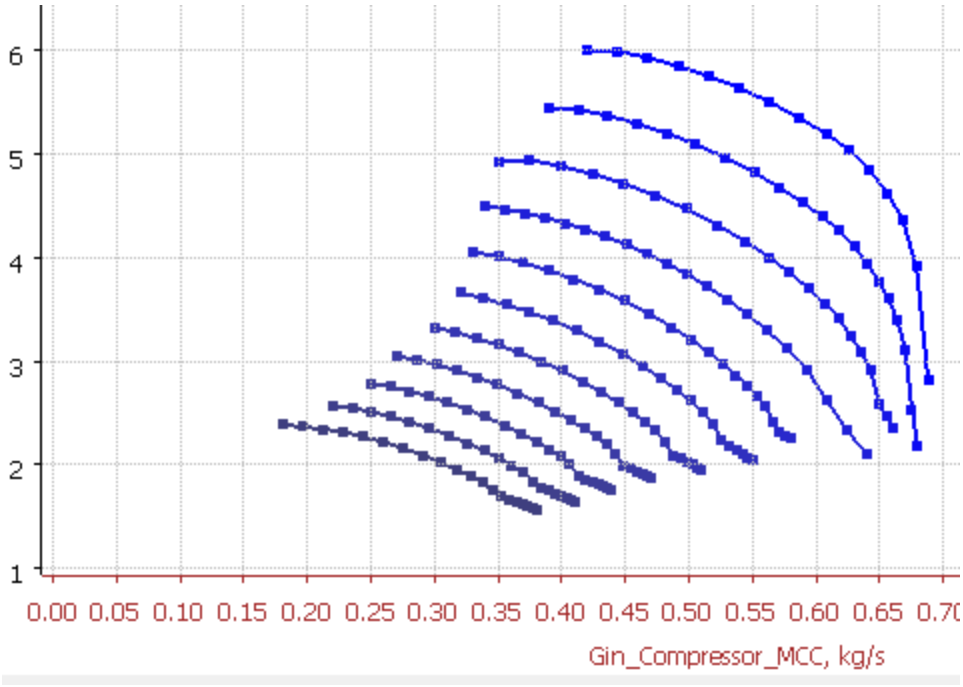

Figure 6: Compressor representative performance map at design inlet conditions

Turbine

The turbine is a radial turbine specifically designed with AxSTREAM to convert the thermal energy of the fuel cell exhaust into mechanical work as addition to the electromotor driving the compressor. The turbine is integral to the overall engine efficiency, particularly in compact and high-performance aviation applications where space and weight are critical factors.

The turbine features a single-stage radial inflow configuration, optimized for high-pressure ratio applications.

At the design point, the turbine operates at a pressure ratio of 4.6. The inlet pressure and temperature at this point are 4.66 bar and 159 °C, respectively. The turbine operates at the same rotational speed as the compressor (56000 rpm), and under these conditions, it delivers a power output of 124kW with an isentropic efficiency of 92%.

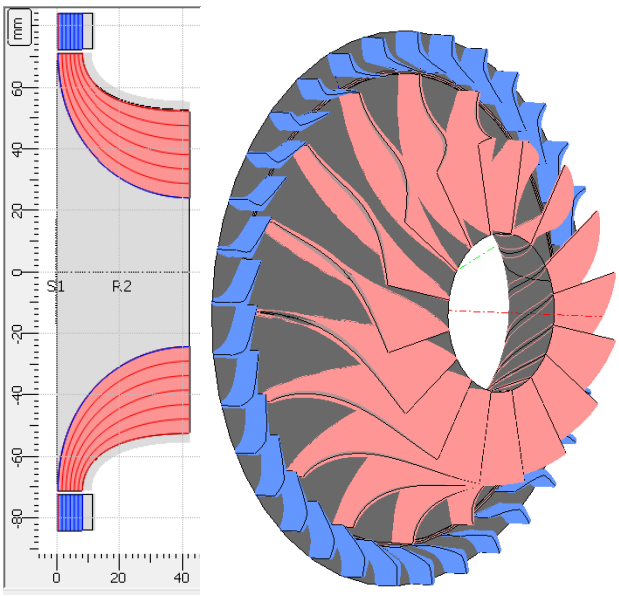

Figure 7: Meridional view and 3D rendering of turbine flow path

The design point is carefully selected to ensure that the turbine operates at peak efficiency during the most demanding phases of flight, such as takeoff and climb. To further elaborate on this point, the turbine flow-passing capability is governed by Stodola's Law of the Ellipse (Dixon, 2005)[5] which says that beyond the critical pressure ratio where the flow through the nozzles becomes sonic, the turbine is choked and the only way to increase mass flow passing capability is by increasing the inlet density and therefor pressure. Understanding this fact and accounting for the fact that it is necessary to maintain stable operation of the compressor, it was clear that the maximum mass flow through the turbine occurs at ground conditions where the air is most dense. At these conditions, the turbine is subjected to the highest thermal and mechanical loads, and its design must ensure reliable operation without compromising performance. Radial-inflow turbines are able to maintain high efficiency and stable performance across a wide range of operating conditions. This includes adapting to changes in altitude, ambient conditions, and engine load, all of which can significantly impact turbine's operating environment. The wisdom of the choice of design point condition and favorability of the design is validated by the results of the simulation, which show the turboexpansion isentropic efficiency is maintained above 86% at all operating points across the entire load range, altitude range from ground to 5400m, and Turbocompressor operating speed range from 38kRPM to 62kRPM.

FUEL CELL

A fuel cell model was utilized as part of the study. This fuel cell was assumed to operate at a constant 80 °C and this was ensured by configuring the thermal management system, to be discussed in a forthcoming section, to control the heat dissipation in a way that guaranteed maintenance of the required temperature. Certain properties were specified for both an individual

[5] (Dixon, 2005)

fuel cell, as well as the overall fuel cell stack. These fixed properties are shown in Table 2. The fuel cell was assumed to utilize 100% of the inlet fuel with any "real" excess going through an H_2 recycle loop, whereas a lower percentage of the oxygen in the oxidizer branch was assumed to be utilized (i.e. there is excess air flow through the fuel cell). The pertinent parameter is called fuel/air equivalence ratio (ϕ) and is always less than unity.

Table 2: Fuel Cell Properties

Property	Value
Single Fuel Cell Area [m^2]	0.1
Catalyst-Specific Area [cm^2/mg]	1000
Catalyst Loading [mg/cm^2]	0.5
Membrane Humidity Level	100% Humidified
Membrane Thickness [mm]	0.178
Cell Number - Stack	2450
Operating Temperature [°C]	80

The IV curve and Power curve for this fuel cell are shown in Figure 8 and Figure 9, respectively. When generating these curves, the fuel cell pressure and oxygen utilization were assumed to be fixed at 0.475 MPa and 0.542 respectively. However, in the complete system model, these fixed parameters will vary due to the influence of the overall system performance (and primarily influenced by the turbocompressor performance). This will cause the fuel cell performance to shift slightly from what is shown in the below figures.

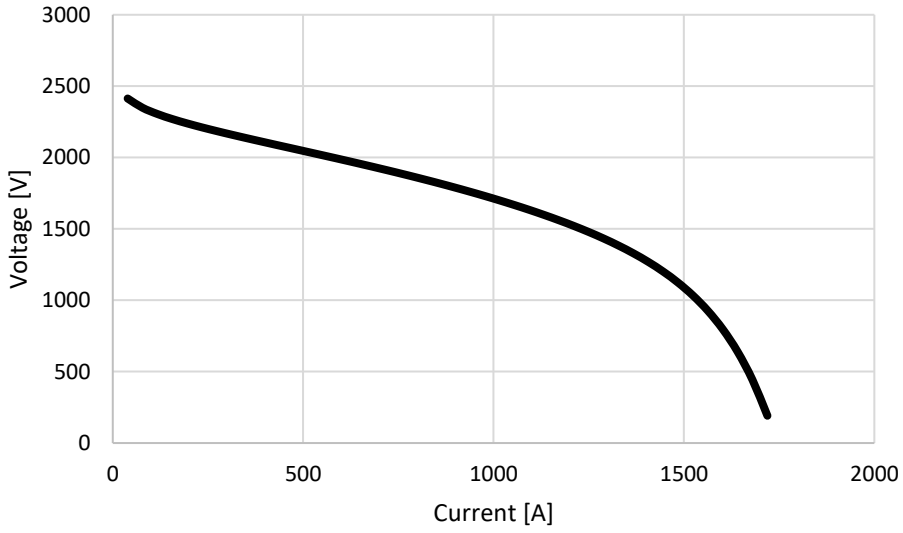

Figure 8: Fuel Cell IV Characteristic at Nominal Conditions

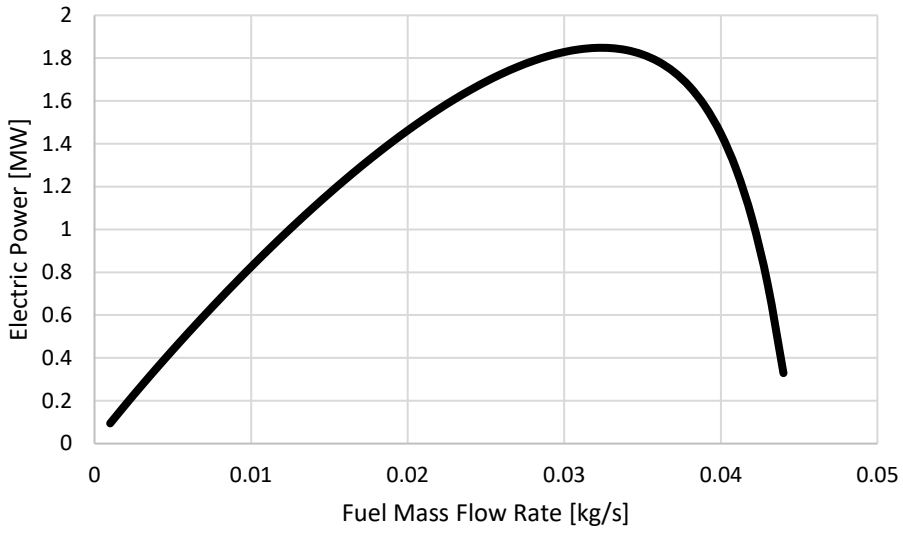

Figure 9: Fuel Cell Power Curve at Nominal Conditions

The curves above were generated by running an isolated submodel of the exact fuel cell design utilized in the full model and show that the simulation model does indeed respond to boundary conditions, as expected by physical principles.

THERMAL MANAGEMENT SYSTEM

A 1D model of the thermal management system was implemented as part of the cosimulation model in AxSTREAM System Simulation. The coolant (an antifreeze mixture of 20% ethylene glycol, 80% water) is used to first absorb heat across the fuel cell coolant channels. A portion of the hot coolant then rejects the absorbed heat across an air-cooled radiator, while the rest of the coolant is bypassed around the radiator, in order to maintain the fuel cell stack temperature at its optimum condition. The cold coolant then mixes with the bypassed coolant and returns to the pump, thus completing the cooling loop. The schematic of the 1D thermal management system is shown in Figure 10. The fuel cell coolant channels are highlighted by the green box, while the radiator is highlighted by the red box. Note that this figure does not show the schematic of the entire aero engine model, but instead isolates just the thermal management portion of the model, for ease of visualization.

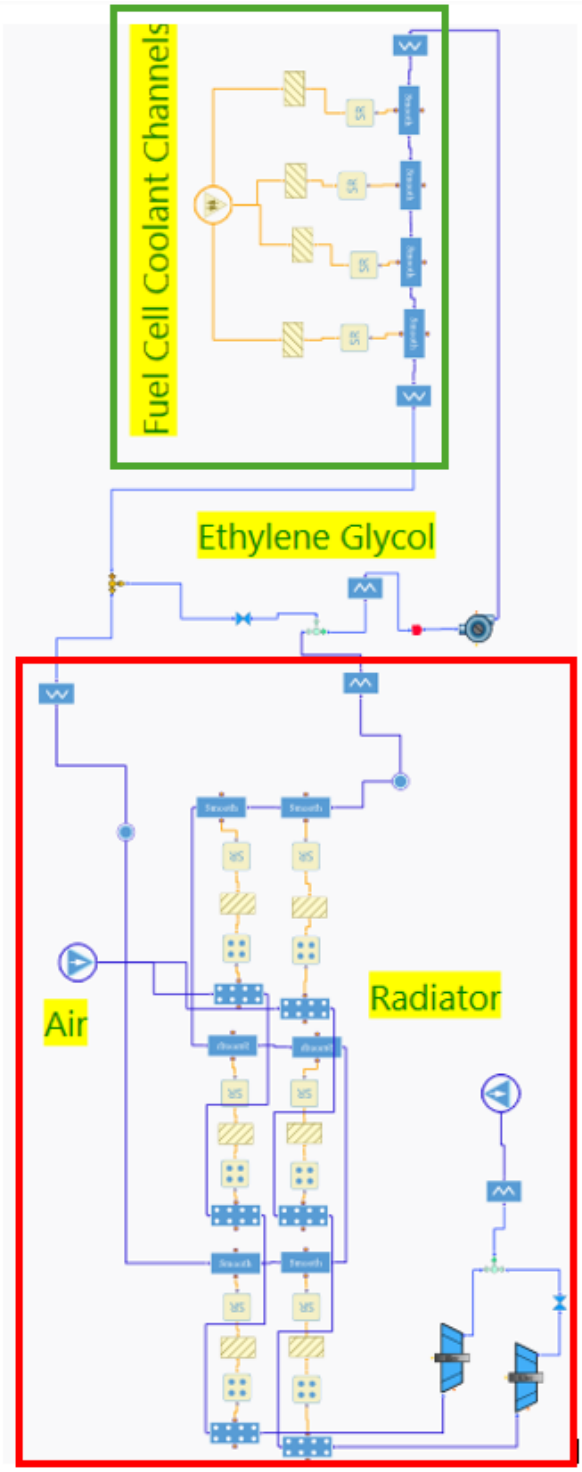

Figure 10: Schematic of Thermal Management System Model with a green box (top) showing the fuel cell cooling channel model and red box (bottom) showing the rejection heat exchanger which typically is called a radiator

Fuel Cell Coolant Channels

To understand the fuel cell coolant channels, one should first understand the architecture of the fuel cell stack. A 2D representation of a portion of the fuel cell stack is shown in Figure 11. Each cell consists of a membrane-electrode assembly and a bipolar plate. The membrane electrode assembly consists of the anode, proton exchange membrane (PEM) sandwiched between porous catalyst and gas diffusion layers, and cathode. Each bipolar plate has channels to allow for the flow of fuel (hydrogen) and oxidizer (air). For a particular cell, fuel is channeled to the anode and oxidant is channeled to the cathode. At the anode, hydrogen is split into hydrogen ions and electrons. The PEM allows only the positively charged ions to pass through to the cathode, while the negatively charged electrons must travel along an external circuit to the cathode. At the cathode, hydrogen ions and electrons combine with oxygen to form water, which is then exhausted from the fuel cell via the cathode gas flow channels. Multiple cells are stacked one after another to form a fuel cell stack. This electricity generating process generates heat which needs to be rejected from the stack. Therefore, for every several cells, a cooling plate is implemented where a coolant is used to absorb the heat from the fuel cell. The number of coolant channels and the number of cooling plates may be adjusted as part of the design of the cooling system.

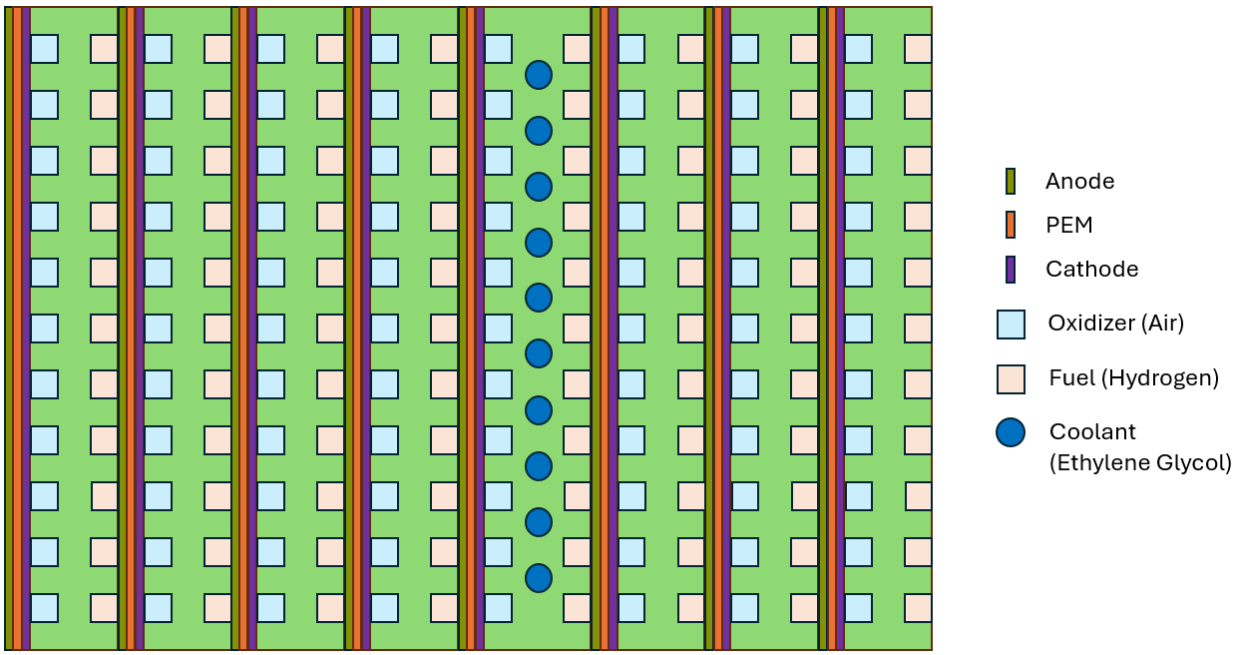

Figure 11: 2D Representation of Partial Fuel Cell Stack

To better visualize the fuel cell architecture, a 3D representation of a portion of the fuel cell stack is shown in Figure 12, while a zoomed in view is shown in Figure 13. The bipolar plate is shown in gray, the coolant plate is shown in bright green, while the anode, PEM, and cathode are shown in dark yellow, orange, and purple, respectively. These figures only show a portion of the stack, the fuel cells and coolant plate would repeat as the stack grows larger.

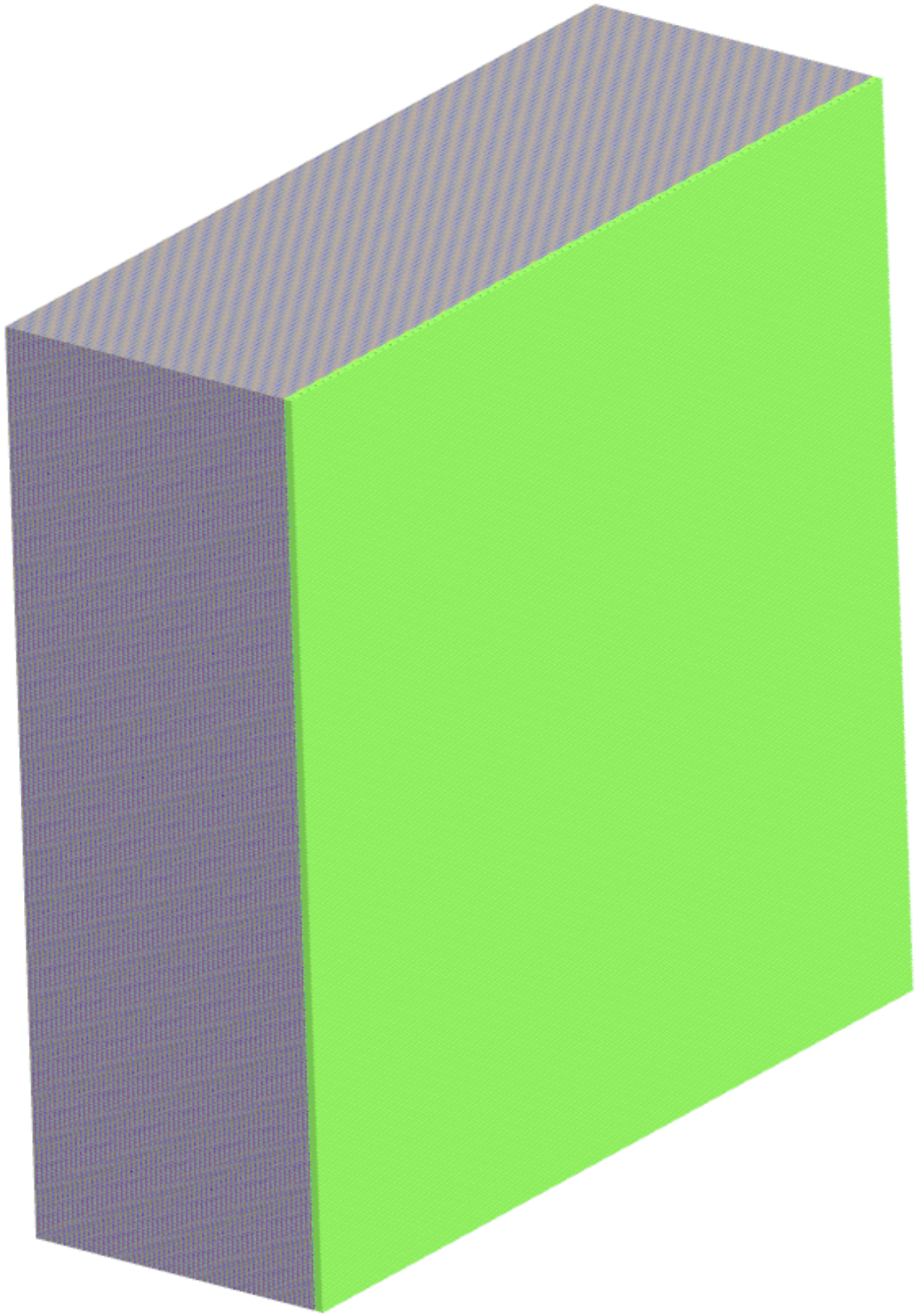

Figure 12: 3D Representation of Partial Fuel Cell Stack

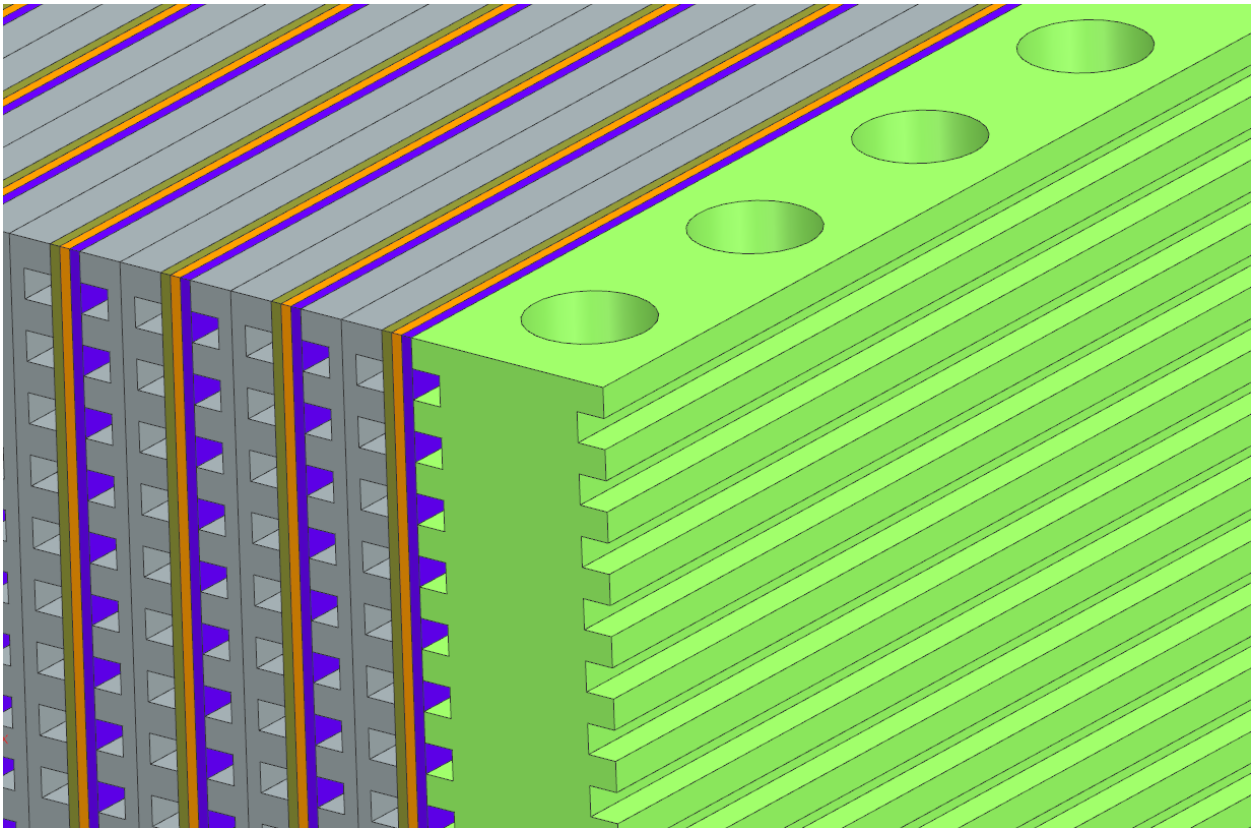

Figure 13: 3D Representation of Partial Fuel Cell Stack – Zoomed In View

The portion of the 1D model for the fuel cell coolant channels is shown in the green box in Figure 10. The fluid channel components are in blue, while the thermal elements are in yellow. The coolant enters from the top into a flow resistance element. This represents the piping going between the pump and the coolant channels. A resistance coefficient of zero was specified for this element, so no pressure drop was modeled prior to the coolant channels. However, this resistance coefficient could later be tuned if desired to model the pressure drop along the coolant piping and inlet manifold, which is expected to be insignificant compared to the intrachannel pressure drop.

After the first resistance coefficient, the flow goes into the first smooth pipe elements. 3500 pipe instances were specified in each smooth pipe component. This represents the inlet flow splitting evenly amongst 3500 parallel cooling channels. This number of pipe instances was selected to ensure both sufficient heat transfer surface area and reasonable coolant flow velocities. The four smooth pipe elements in series represent the channels being discretized along their length for better modeling accuracy of the heat transfer change from the top to the bottom of the fuel cell.

To determine how the cooling channels are divided up, the fuel cell geometry again must be considered. The fuel cell element has a fuel cell area specification of 0.1 m^2. If we consider each fuel cell to have a square shape, this means that the fuel cell would be approximately 316 mm wide by 316 mm high. Assuming the coolant channel spans the entire width of the fuel cell, and

since there are four pipe elements in series, each pipe element had a specified channel length of 79 mm.

A rectangular cross section of 2 mm x 2 mm was specified for the cooling channels. It was also assumed that there is 2 mm of spacing between each cooling channel. Given the 316 mm height of the fuel cell, this means 79 cooling channels can fit in a single cooling plate. Since 3500 cooling channels were selected, this means that at least 45 cooling plates would be required with this design. The fuel cell element specified 2450 fuel cells in the fuel cell stack. This means that each cooling plate is responsible for the cooling of approximately 55 fuel cells. A summary of the fuel cell coolant channel geometry is provided in Table 3. Note that while this model represents one coolant channel arrangement, the model parameters could be adjusted to model different cooling channel geometries in future analyses.

At the outlet of coolant channels is another fluid resistance element. This models the flow between the outlet of the fuel cell coolant channels and the inlet of the radiator. Currently, the resistance coefficient in this element is set to zero. However, this value can be adjusted to model different pressure drops between the fuel cell and radiator.

Table 3: Fuel Cell Coolant Channel Properties

Property	Value
Fuel Cell Area [m^2]	0.1
Fuel Cell Width [mm]	316
Fuel Cell Height [mm]	316
Number of Cooling Channels	3500
Cooling Channel Width [mm]	2
Cooling Channel Height [mm]	2
Cooling Channel Length [mm]	316
Spacing Between Cooling Channels [mm]	2
Cooling Channels per Cooling Plate	79
Minimum Number of Cooling Plates	45
Number of Fuel Cells in Stack	2450
Fuel Cells Cooled per Cooling Plate (approx.)	55

When analyzing a solution to the system model, at the inlet and outlet of each 1D element, the thermodynamic fluid properties are calculated. Additionally, nondimensional parameters such as Reynolds number and Prandtl number are calculated. Based on these calculated parameters, the Darcy friction factor, resistance coefficient, and pressure drop can be calculated for each 1D element, as shown in Equation 3.

$$\Delta p = \frac{\zeta \rho \omega^2}{2}$$

$$\zeta = \frac{\lambda l}{D_h} \tag{3}$$

$$\lambda = f(Re\,, channel\ type)$$

Where pressure drop (Δp) is a function of frictional resistance coefficient (ζ), density (ρ), and mean flow velocity (ω). ζ in turn is a function of Darcy friction factor (λ), channel length (l), and hydraulic diameter (D_h). Finally, λ is a function of Reynolds number (Re) and the channel shape factor (i.e. channel type).

To model heat transfer into the 1D elements, thermal elements were used (the yellow components of fuel cell coolant channel portion of Figure 10). First, a thermal boundary element (left-most thermal element of the fuel cell coolant channel portion of Figure 10) was used where the heat rejected from the fuel cell is supplied evenly along the cooling channels.

A wall conduction element was then used to model the heat conduction through the walls of the cooling channels. The wall thickness was specified as 1 mm, based on the spacing of the cooling channels. The cooling channels were assumed to be made of Aluminum 6061. The heat transfer across the wall is calculated based on Equation 4.

$$\dot{Q} = \left(\frac{k}{0.5t}\right) A_s (T_s - T_{av}) \tag{4}$$

Where k is the average thermal conductivity, t is the wall thickness, A_s and T_s are the surface area and temperature of the wall surface in question, and T_{av} is the average temperature across the wall.

Next, the convective heat transfer was modelled for each piping element using a convection element. Based on the Reynolds numbers and Prandtl numbers calculated in the 1D elements, the convective heat transfer properties were calculated. While the Dittus-Boelter convection correlation[6] may be a more typical choice, the Reynolds number in the cooling channels were below the recommended range of the Dittus-Boelter correlation. Because of this, the Sleicher-Rouse convection model was selected instead[7], which is shown in Equation 5.

[6] (Incropera, Dewitt, Bergman, & Lavine, 2011)
[7] (Sleicher & Rouse, 1975)

$$Nu = 5 + 0.15Re^{a}Pr^{b}$$

$$a = 0.88 - \frac{0.24}{4 + \mathrm{Pr}} \tag{5}$$

$$b = \frac{1}{3} + 0.5e^{-0.6\mathrm{Pr}}$$

Where Nusselt Number (*Nu*) is a function of Reynolds Number (*Re*) and Prandtl Number (*Pr*).

Across the conduction and convection elements, the temperatures are calculated. Thus, the temperature distribution from the coolant to the outer wall of the coolant channel can be determined.

Radiator

A 1D shell-and-tube radiator was modeled where heat from the coolant is rejected to ambient air. The coolant tubes consist of three sets of parallel tubes in series. Cold ambient air is blown across the coolant tubes to cool the coolant. The total volumetric flow rate of air was specified at 12 m^3/s. This flow rate was chosen to ensure sufficient air temperature rise while still maintaining a low drop in air pressure across the radiator. The heat exchanger model was discretized into a 2 by 3 arrangement; discretized into two sections in the coolant tube direction and discretized into three sections in the air flow direction (one section for each set of parallel tubes). The schematic of the radiator model is highlighted by the red box in Figure 10 while a diagram of the fluid flow path and discretization through the radiator is provided in Figure 14.

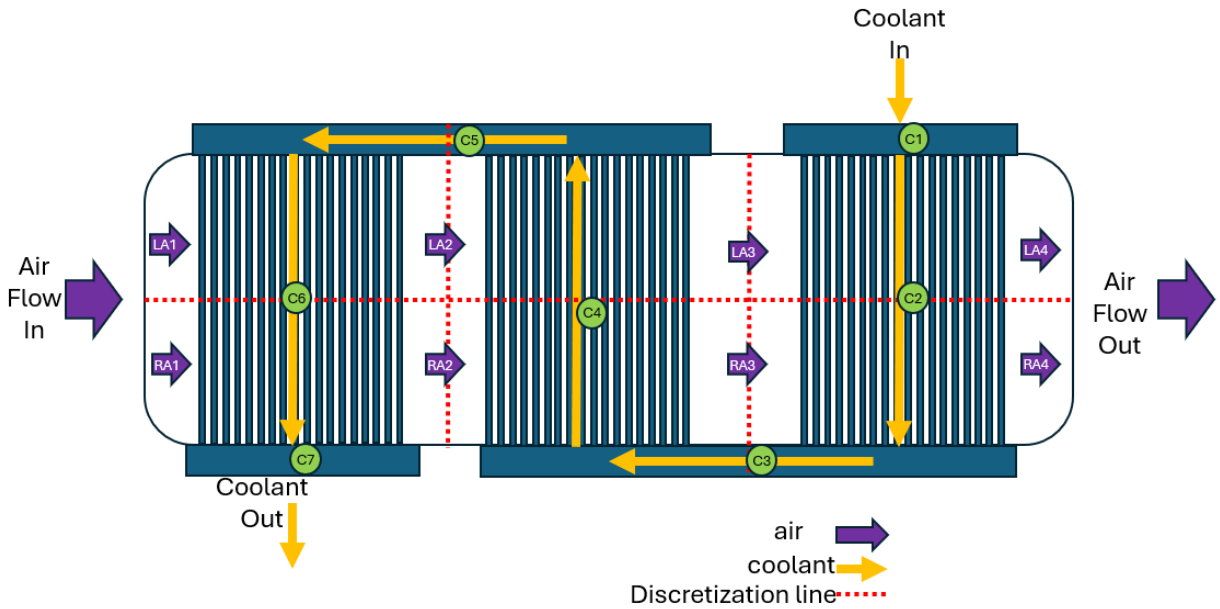

Figure 14: Discretization of Flow Through Radiator

The coolant tubes are arranged in three sets of 5000 tubes (15000 tubes total). The tubes are discretized lengthwise into two segments of 500 mm (1 m total length). Each tube has a 2 mm internal diameter and a 2.5 mm external diameter. Each set of 5000 tubes is arranged such that there are 250 tubes across the air flow and 20 tubes along the air flow. When the three tube sets are accounted for there is a total of 60 tubes along the air flow. The longitudinal pitch and cross pitch of the tubes were both set to 5 mm, thus the space between the tubes was equal to the width of the tubes. A summary of the radiator geometry is provided in Table 4.

Table 4: Radiator Properties

Property	Value
Number of Tubes	15000
Tube Length [mm]	1000
Tube Inner Diameter [mm]	2
Tube Outer Diameter [mm]	2.5
Tube Longitudinal Pitch [mm]	5
Tube Cross Pitch [mm]	5
Tubes Across Air Flow	250
Tubes Along Air Flow	60

As seen in the radiator portion of Figure 10, there are three thermal elements modelling the heat transfer between the coolant and the air. The Sleicher-Rouse convection model was used to model the internal convection between the coolant and the inner tube wall (see Equation 5). This convection component used fluid properties calculated in the 1D pipe elements. Next, a thermal wall element was used to model the conduction through the tube walls (see Equation 4). The

tubes were assumed to be made of Aluminum 6061. Finally, the external convection on the shell side was modelled based on the fluid properties calculated in the Tubular Heat Exchanger – Shell Side 1D component. The Isachenko equation[8,9] was used to model the Nusselt number of the air flowing across the tube banks, as shown in Equation 6.

$$Nu = CRe_d^n Pr_f^{0.33} \varepsilon_s \varepsilon_n \varepsilon_\varphi \left(\frac{Pr_f}{Pr_\omega}\right)^{0.25} \quad (6)$$

Where Nusselt number (Nu) is a function of constants (C = 0.26, n = 0.65), Reynolds number by outer tube diameter (Re_d), Prandtl numbers by fluid temperature (Pr_f) and wall temperature (Pr_ω), correction for pitch (ε_s), correction for tube rows (ε_n), and correction for angle of attack (ε_φ).

Additional Coolant Loop Specifications

All the flow from the coolant pump goes through the fuel cell coolant channels. The flow then splits, with some of the flow going through the radiator and the rest bypassing the radiator. These two fluid branches eventually recombine prior to reentering the pump. Bypassing more of the flow around the radiator will make the inlet temperature to the pump and fuel cell hotter. To control the coolant temperatures and split ratio, first it should be noted that by energy conservation, the energy going into the coolant across the pump and fuel cell must equal the energy being rejected by the coolant across the radiator. Second, it was specified that the average outer wall temperature of the fuel cell coolant channels must equal the temperature specification of the fuel cell component (80 °C). Based on these principles, the temperature distribution and split ratio of the coolant could be determined. This effectively models an active thermal control scheme that uses a temperature control 3-way valve or a 3-way valve actuated by feedback control from a measured fuel cell stack temperature sensor.

When considering the operating parameters of the coolant pump, the different operating conditions of the system must be considered. At ground conditions, the air temperature will be at its hottest. This air temperature may vary depending on where the system is being operated. When the ambient temperature gets hotter, more coolant needs to be diverted across the radiator to sufficiently lower the coolant temperature. Therefore, the total coolant mass flow rate should have some margin to allow for the additional coolant needed at these hot locations. Based on this, a mass flow rate of 12 kg/s was selected for the cooling pump. Notice in Table 5 how the coolant split ratio is low at typical ground conditions, but at hot ground conditions the split ratio is nearly one with almost all the flow going across the radiator.

When considering the coolant loop pressures, the largest ambient pressure the system would experience is at ground conditions (101 kPa). The lowest pressure in the coolant system will be at the inlet of the pump. This low coolant pressure was fixed at slightly above the ground ambient pressure (110 kPa) to ensure that the coolant loop would remain above the ambient pressure at all operating conditions and would not need to be maintained under partial vacuum.

[8] (Orlov, 2013)
[9] (Akmen, 2007)

The required pressure rise of the pump is based on the pressure drop of the coolant across the rest of the coolant loop. The pump was assumed to operate with 90% isentropic efficiency across all conditions, although the relatively small power draw for pumping makes this choice nearly inconsequential.

Another consideration of the cooling system is the air flow across the radiator. The inlet conditions will vary based on ambient conditions. Certain parameters such as the air temperature and density will drop at higher altitudes. Since a constant volumetric flow rate of air was assumed across all conditions, this means that the air mass flow rate decreases at high altitudes. To counteract this, volumetric flow rate should be set sufficiently high to provide ample cooling at all conditions. However, the flow rate shouldn't be too high, or else there will be large air pressure drops across the radiator. Based on these factors, a volumetric flow rate of 12 m^3/s was chosen. This flow rate resulted in an air pressure drop of approximately 3 kPa across the operating range. The balancing of the air flow parameters can be seen in Table 5.

A comparison of the coolant system performance at different operating conditions is provided below in Table 5.

Table 5: Thermal Management System Performance – Multiple Operating Conditions

	Take Off	Take Off – Hot Climate	Low Altitude Cruise	High Altitude Cruise
Operating Conditions				
Altitude [m]	0	0	50	5400
Atmospheric Pressure [kPa]	101.325	101.325	100.726	51.226
Atmospheric Temperature [°C]	15	34	14.7	-20.1
Fuel Cell				
Aspiration Air Flow Rate [kg/s]	0.849	0.772	0.861	0.549
Heat Rejection [kW]	466	475	464	515
Coolant Pump				
Mass Flow Rate [kg/s]	12	12	12	12
Inlet Temperature [°C]	66.5	66.3	66.6	65.1
Fuel Cell Coolant Channels				
Coolant Inlet Temperature [°C]	66.6	66.3	66.6	65.1
Coolant Outlet Temperature [°C]	76.3	76.2	76.3	75.9
Coolant Split Ratio	0.211	0.945	0.208	0.175
Radiator				
Coolant Mass Flow Rate [kg/s]	2.53	11.34	2.50	2.09
Coolant Pressure Drop [kPa]	3.37	13.11	3.35	3.30
Coolant Outlet Temperature [°C]	29.8	65.7	29.3	13.4
Air Outlet Temperature [°C]	46.5	68.2	46.2	40.6
Air Volumetric Flow Rate [m^3/s]	12	12	12	12
Air Mass Flow Rate [kg/s]	14.63	13.72	14.55	8.41
Log Mean Temperature Difference	34.3	14.1	34.6	54.5

HOLISTIC SYSTEM SIMULATION MODEL

The turbine and compressor are successfully integrated into the engine model. The compressor and turbine are mounted on the common shaft, directly coupled with an electromotor. This configuration allows for precise control of the shaft's rotational speed and the power input in the turbine-compressor-motor assembly (turbocompressor).

A two stage inline centrifugal compressor is responsible for compressing incoming air to a high pressure before it enters recuperator and subsequently the fuel cell. The compressor's performance is characterized by its pressure ratio and efficiency that are dependent on rotational speed that is controlled by electromotor and mass flow rate that is established by the system.

A radial inflow turbine extracts energy from the exhausts to provide additional power to the compressor and reduce electrical power consumption of the electromotor. Based on the inputs, which for the turbine are inlet and outlet total pressure, turbine inlet temperature and rotational speed, controlled by the electromotor, the efficiency and mass flow rate of the turbine are solved by the turbine model which rounds in a coupled co-simulation with the overall system.

An electromotor provides control over the shaft's rotational speed. The electromotor can adjust the rotational speed to match the desired operational conditions, thereby controlling the performance of both the compressor and turbine and drawing whatever power is necessary from the fuel cell in the balance between the compressor and turbine.

The entire system is simulated as a coupled model, where the interactions between the turbine, compressor, and electromotor are dynamically represented. A key feature of our work is that the compressor and turbine flow paths are designed in detail with full geometry resolution of the aerodynamic surfaces so that aerodynamic performance can be simulated. Additionally, the fuel cell is defined as a 1D model, which means that important design parameters such as catalyst loading, fuel cell area, and stacking are defined and used in simulating the performance of the fuel cell in addition to physical parameters. Finally, the thermal management system is also defined at the 1D level as a detailed thermo-fluid network. It is important to include the thermal management system because it determines the equilibrium temperature of the fuel cell stack. This temperature, in addition to the reactant pressures, equivalence ratio, and fuel cell design parameters determine the fuel cell performance via the 1D model.

The turbomachinery is directly coupled with the system and forms, effectively, a coupled set of nonlinear simultaneous equations that are solved iteratively. The inputs to the compressor are the inlet pressure and temperature, air mass flow rate and rotational speed, while the outputs to the system are the outlet pressure and isentropic efficiency, which determines the outlet temperature and enthalpy. The inputs to the turbine are the inlet temperature and pressure, the outlet pressure, which is the ambient pressure, and the rotational speed. The turbine submodel solves and outputs to the system model the mass flow rate and isentropic efficiency which determine the outlet temperature and enthalpy. It should be observed that the input pressure of the turbine submodel is determined by the output of the compressor submodel while the input flow rate of the compressor submodel is determined by the output of the turbine submodel. The system components are holistically coupled to the system and to each other, and the converged mathematical solution thus satisfies convergence of all subcomponents and the overall system determines the solution to the complete system. The following section will attempt to elucidate the physical interactions of the components further while focusing on the system control aspects in steady state.

SYSTEM CONTROL

It is important to emphasize the method of specifying the simulation parameters. Two paradigms of engineering simulations are commonly called "design mode" and "analysis mode." In design mode, input parameters of the simulation can be chosen by the designer according to the goals of the simulation. For example, in the present model, it may be of interest to determine the effect that the compressor pressure ratio, or flow, or the recuperator exit temperatures, or any other parameter that may be affected by component design choices, may have on the overall power specific fuel consumption of the engine or some other performance indicator of interest. In this case, it is possible to specify the inputs of the simulation directly to perform the analysis and obtain results. In fact, in the nominal design of the particular case which is the subject of this paper, precisely these types of studies were performed to arrive at a nominally appropriate power system design for the chosen application. It should be emphasized that in design mode, inputs of

the simulation are relatively flexible and need not be actual physically controllable parameters. A quantity such as pressure ratio and flow rate of a compressor depends on the design of the compressor, so design mode simulations are typically carried out specifically for the purpose of design – especially the design of subcomponents within the system.

On the other hand, in analysis mode simulations, the designs of all the components are fixed. The unique property of analysis mode simulations is the choice of input parameters to the simulation is more restrictive in comparison to design mode simulations. The availability of choices that are present depend on the level of fidelity of the simulation system. In the present work, we wish to develop a digital twin of a realistic system, and need to consider the components of the system whose performance characteristics will be the most variable under change in operating conditions. These will be the turbomachinery that forms the aspiration system and the thermal management system of the fuel cell that enables regulation of temperature under various power levels and efficiencies. Thus, to faithfully evaluate the system behavior under various operating conditions, it is necessary to have some design details of the compressor and expander so that their performance is understood. As described in a previous section, these components were designed. To summarize the discussion with emphasis on system specification, it is emphasized that instead of specifying a compressor flow rate, or pressure ratio, or turbine power production, and many other parameters that are not physically controllable, in the digital twin we specify only the rotational speed of the aspiration turbomachinery train, which then solves for the power balance, flow rates, and pressure boundaries through the co-simulation interaction of the components within the overall system, as was described in the previous section. The system control inputs and major responses are shown in Figure 15.

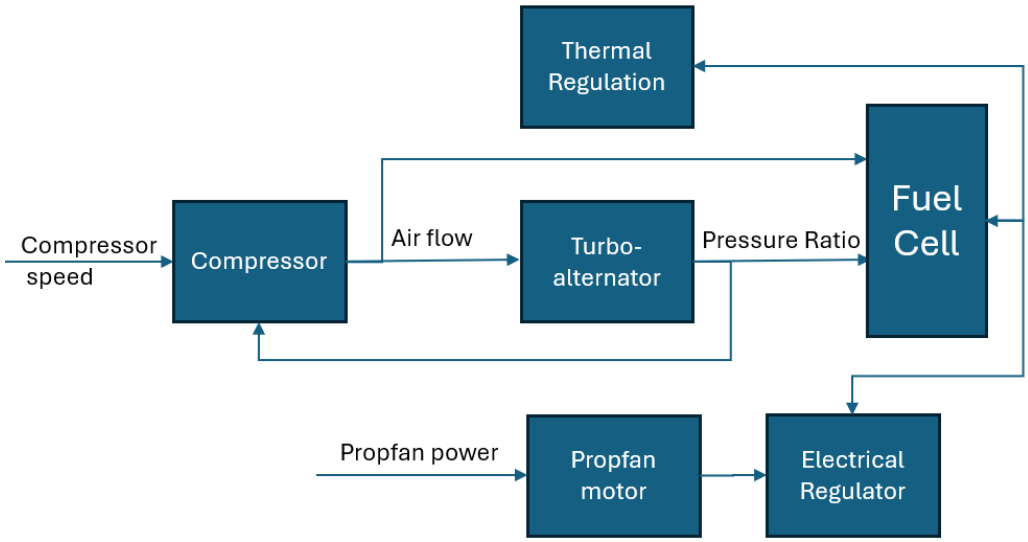

Figure 15: Block diagram of the control input signals and plant transfer function processes

The reader may at this point scrutinize why particular inputs that have been chosen are deemed as directly controllable, and indeed this is a critically important question that will be addressed shortly. Before doing so, it is useful to examine the parameter interactions in the physical model. As can be seen, the direct control inputs into the model are the compressor speed and the propfan motor power demand. The other direct simulation inputs are the aircraft altitude, temperature

offset (vs. ambient conditions at the specified altitude), and flight velocity – which are not control inputs but operational inputs even though from the perspective of numerical simulation they are indistinguishable. These inputs tell the simulation under what condition the engine is operating. All other parameters are therefore determined by the simulation. The conceptualization of how the subsystems interact holistically can be enabled by following the diagram of Figure 15 and is described in the forthcoming paragraph. It must be noted that the description focuses on the physical processes rather than the mathematical and numerical methodology of solving the full system, which has been described in a previous section.

The aspiration turbomachinery rotational speed is input as the control (labelled compressor speed). The compressor rotation induces air flow into the system. The amount of air flow is governed by both the speed (direct input) and the outlet pressure which is a feedback of pressure ratio from another part of the system (the turboexpander). The airflow then determines the equivalence ratio, which is one of several key inputs into the fuel cell sub-model, along with the reactant pressures and load demand. The fuel cell produces an exhaust composition at the cathode and a thermal waste heat product based on these inputs. The exhaust fluid stream then goes into the turboexpander, which has a volumetric flow swallowing capacity and efficiency characteristic that is determined by the aerodynamic design of the flowpath, and which therefore will generate a backpressure based on the flow rate that ultimately sets the outlet pressure of the compressor and the fuel cell cathode reactant pressure (the anode reactant, or hydrogen, pressure is equalized to the cathode). Similarly, the thermal waste heat will cause the thermal management system to modulate its own simulated control scheme to regulate the fuel cell temperature. While the above discussion focused on following parameter “signals” as they interacted between components, mathematically the system is effectively a numerical solution of simultaneous non-linear equations.

As was promised, it is prudent to expound and justify the chosen input parameters as directly controllable. As was previously stated, the choices of what parameters may be considered directly controllable in analysis mode system simulation depends on the model fidelity details. In the present work, it was deliberately chosen to have relatively high fidelity on the fluid and thermal components of the system and relatively low fidelity (0D) on the electrical system components. Therefore, it is understood that in the physical system, an electrical power system regulator will include rectification, inversion, and variable frequency drive electronics, as well as the digital and analog controllers that enable regulation of electrical voltage, current, and frequency in a multiphase system that will enable proper electrical inputs to the two electrical motors in the system and enabling the acceptance of a DC input from the fuel cell while regulating the impedance for proper load control. All these features are only modelled as 0D electrical efficiencies. Thus, it is reasonable to simplify all the interesting nuances of the electrical and electronic system into a single block such that an electronic control input can be a frequency input to a motor. We assert that it is a reasonable assumption that the electrical regulator will enable input of a digital speed control setpoint and will subsequently regulate an input AC voltage and frequency characteristic in an internal feedback control loop to stabilize at the setpoint speed of the turbocompressor so long as enough power is available from the system power balance. Similarly, it is reasonable to assume that a digital setpoint power input can be given to the same controller to drive the main propulsion fan at whichever speed and torque is necessary. It is recognized that various types of propfans can be utilized, each of which will have

their own speed versus power and propulsor efficiency characteristics. For the purposes of the present work, we wish only to holistically design and simulate a full power system for the aircraft application without needing to rely on assumptions about exactly what type of propulsor is used.

It is clear now that given certain boundary conditions, namely the altitude, speed, and outside temperature (applied as an offset to the standard ISA tables[10]), the direct control inputs to the power system are power demand to the main drive and the turbocompressor speed. Fundamentally, the aircraft operator typically desires a single control actuator for the engine. Such a control is typically called the throttle, which must be distinguished from the technical thust of the propulsion system that is the propulsive force. The control throttle is more correctly understood as a fractional power setting, where maximum control throttle corresponds to the maximum power capability under the current operating state while minimal throttle corresponds to idle, which in the case of a fuel cell system is actually close to zero power. Therefore, the extra input control of turbocompressor speed is anticipated to be regulated internally to the power system by the FADEC. Thus, a key useful feature of the digital twin simulation system is to determine appropriate control laws to enable maximum efficiency operation of the engine by appropriately controlling the turbocompressor speed for all possible operating conditions and operator control throttle inputs.

SIMULATION RESULTS AND ANALYSIS

Once the full simulation model had been completed and validated, we executed multiparameter sweep analyses to obtain useful inferences about the operational characteristics of the system and understand gain inferences, as described, about developing a control algorithm for a FADEC system to regulate internal engine parameters. It should be emphasized that the breadth of what was done is just an example of the much greater amount of analytical studies or post processing steps that may be taken to fully understand the system under study and is intended to showcase the power of holistic system modeling and digital twin creation.

Three sets of multiparameter sweeps were conducted and are described in Table 6.

[10] (International Organization for Standardization, 1975)

Table 6: Multirun descriptions

Designation	Swept parameters	Description
Large Parameter Variation Set	• Load • Altitude • RPM	This is an extensive sweep that ultimately simulated 234 successful operating conditions across a set of loads from 40% to 100%, altitudes from ground to cruise, and RPMs from 38kRPM to 60kRPM. It was run for two days on an engineering workstation, and because the inputs extended to regimes that were not able to be physically satisfied, resulted in some "holes" in the dataset
Ground Parameter Sweep	• Load • RPM	This was limited to ground altitude and intentionally zero vehicle velocity and swept load and turbocompressor speed. It ran on a laptop and took less than a single workday for the entire multirun.
Cruise Altitude Parameter Sweep	• Load • RPM	This was limited to cruise altitude and cruise velocity and swept load and turbocompressor speed. It ran on a laptop and took less than a single workday for the entire multirun.

The resulting post processing of the simulation data shows system characteristics and suggests control strategies. The first representation of the data is shown in Figure 16, and shows the total system efficiency as a function of turbocompressor speed at three load levels at the ground altitude condition. The system power efficiency is the overall economy metric of the power system and is defined in Equation 7.

$$\eta_{sys} = \frac{\dot{W}_{Eprop}}{\dot{W}_{chem}} = \frac{\dot{W}_{Eprop}}{\dot{Q}_{heat}+\dot{W}_{FCelec}} \tag{7}$$

Unlike the typical turboprop and generally any gas turbine power system, the system power efficiency of a fuel cell in fact increases as load is decreased due to loss mechanism reduction, and this is clear in the figure.

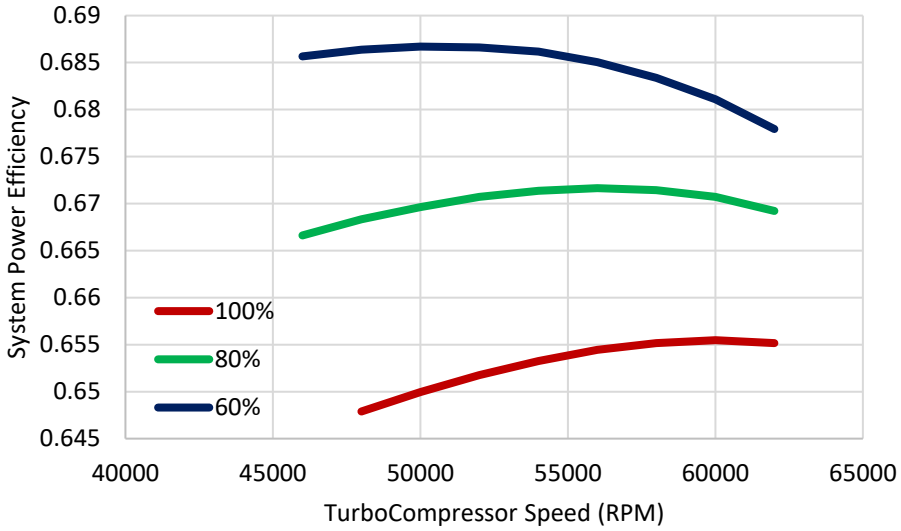

Figure 16: absolute power system efficiency at ground altitude for three load lines

It is also seen from Figure 16 that the load effect on efficiency is significantly larger than the effect from the turbocompressor speed. Nevertheless, there is clearly an optimum speed to operate the aspiration turbo for each power level. It can be reasonably conjectured that the reason for the shape of the curves and an optimum is primarily due to the fact that the chosen architecture has both a recuperator and turboexpander that combined is very effective in recovering the energy that the aspiration compressor puts into the air. If such a recovery system were not present, it is likely that the optimum efficiency would be achieved by operating at the minimum RPM that provided near unity equivalence ratio.

To better resolve the optimum RPM condition, each power level curve was normalized by the maximum efficiency at each power level. The resulting information is presented in Figure 17.

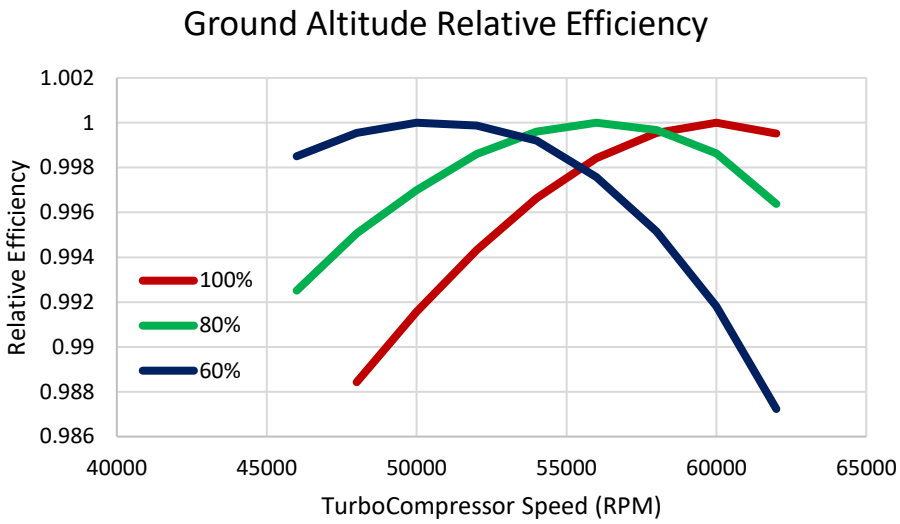

Figure 17: Efficiency at various load lines normalized for each load line at ground ambient conditions, showing optimum turbocompressor speed decreases with load decrease

Thus, we see that at ground altitude ambient conditions, the optimum RPM shifts from 60kRPM at 100% engine power load to about 51kRPM at 60% engine power load. Interestingly, we see the effect on efficiency is relatively low, staying within 2% variance at all conditions. Here again this is likely the effect of our architecture and strong emphasis on energy recovery, which causes the system to be highly efficient.

Performing the same type of post processing for the cruise altitude condition and skipping directly to the normalized presentation, the results are displayed in Figure 18. In the figure, it is seen that generally the trends are similar to those observed for ground altitude, but with a stronger tendency for efficiency maximization at highest turbocompressor RPM. This is expected due to the lower pressures and air density, and therefor the need for higher RPM to achieve the required airflow to maintain equivalence ratios below unity.

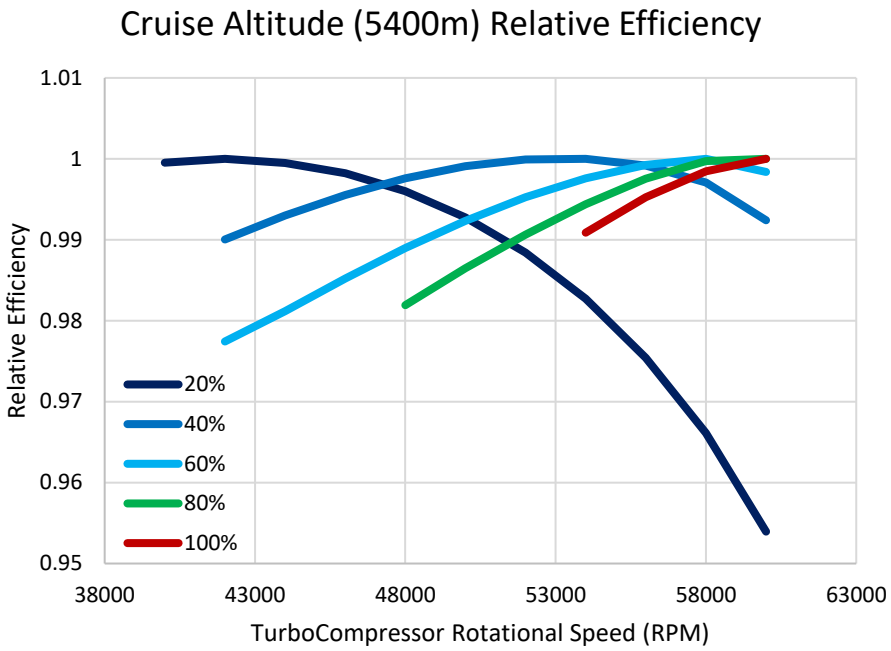

Figure 18: Efficiency at various load lines normalized for each load line at cruise altitude, showing optimum turbocompressor speed decreases with load decrease

Extending this kind of post-processing in a slightly different way, we utilize the entire large parameter variation dataset to produce contour plots showing the effect on absolute efficiency of variation in both altitude and turbocompressor speed for single engine power settings. This is done for 100% engine power (958kW) and 80% engine power (766kW) in Figure 19 and Figure 20, respectively. Generally, it is seen that similar results can be concluded as from the previous analysis – that for higher power levels, it is advantageous to operate near the top rated RPM. Another feature that was not immediately apparent in the previous results but becomes clear is that the overall system efficiency seems to be maximized for both loads near ground altitude. The results are unsurprising, especially for practitioners of fuel cell systems. One key thermodynamic affecting fuel cell power efficiency is the partial pressures of the reactants, with generally higher partial pressures having the effect of reducing concentration losses as the reactant species diffuse through the gas diffusion layer and catalyst past the non-participating species in the air. This has the effect of increasing the efficiency of the fuel cell, and consequently the system.

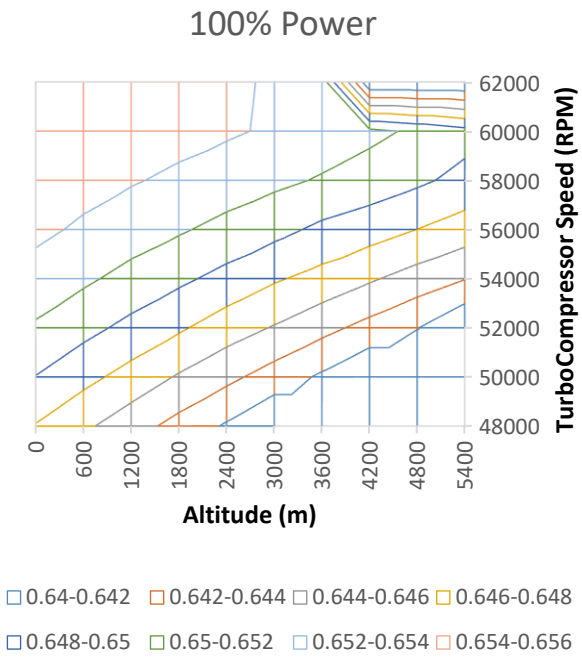

Figure 19: Contour map of total system power efficiency on an altitude and speed dual axes at full engine power

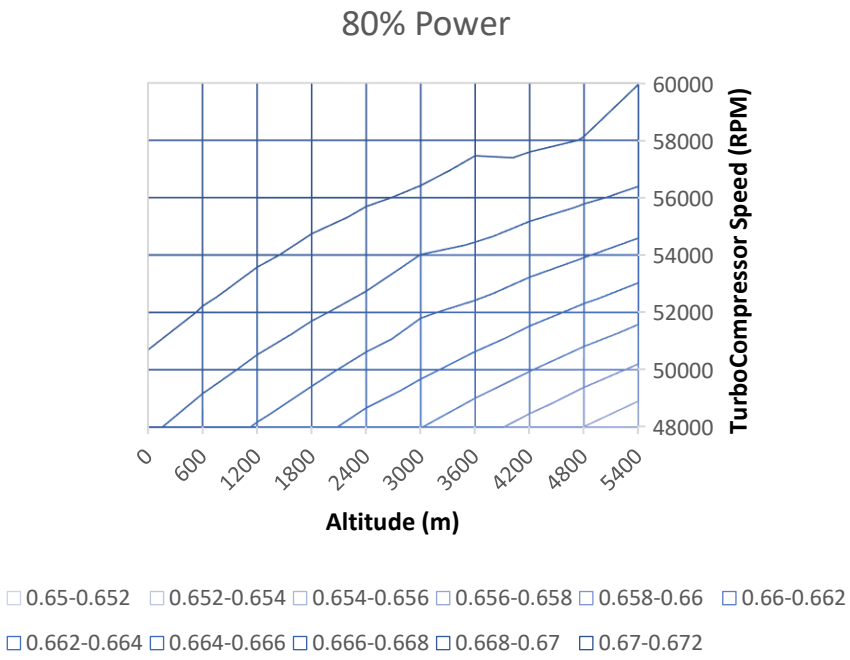

Figure 20: Contour map of total system power efficiency on an altitude and speed dual axes at 80% engine power

Even though the pressure ratio for a particular operating RPM is near constant, the major contributor to the effect is ambient pressure, which decreases with higher altitudes, and therefore causes reduction in absolute pressure of the reactants in the fuel cell as altitude increases. This consequentially causes higher efficiency capability at lower altitudes. However, it must be emphasized that this overall system effect is also a consequence of the energy recovery systems in place for the examined architecture, as was shown in a previous work (Goldenberg, Conser, Joly, & Moroz, 2024)[11]. For systems without recuperated expansion energy recovery, the parasitic load of compression would shift the optimum pressure ratio, and furthermore significantly effect a holistic design of the aspirating compressor.

The effect is shown in detail in Figure 21, where the fuel cell reactant pressure is directly shown as a function of turbocompressor speed at multiple curves of altitude.

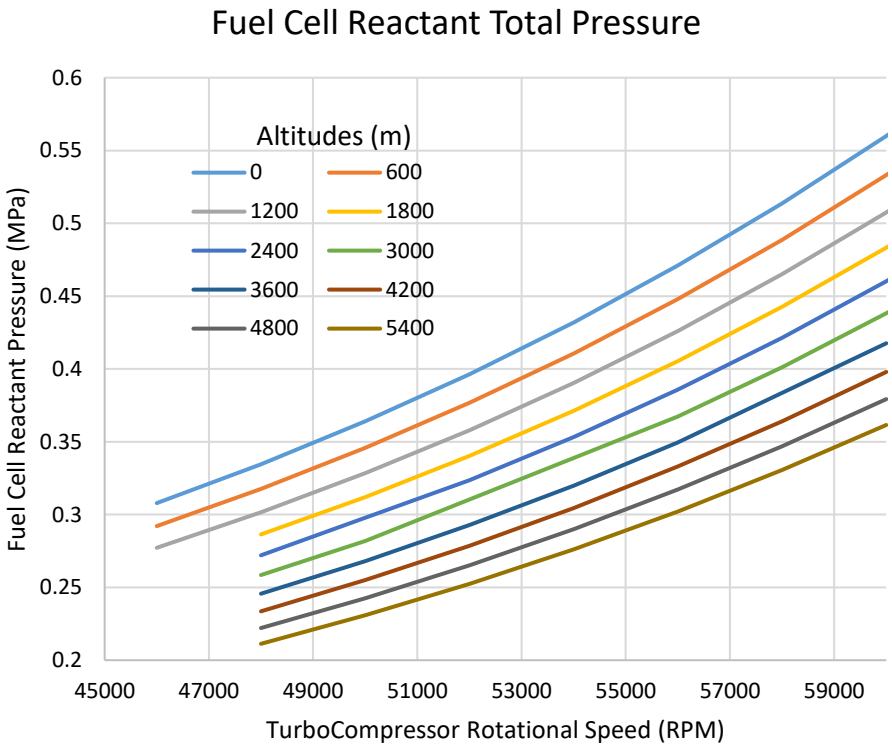

Figure 21: Fuel Cell reactant pressure for a variation of conditions

We see from this that the absolute reactant pressure at the highest altitudes is almost half of the value at sea level, and operation at maximum turbocompressor RPM results in almost the same pressure at high altitudes as operating at significantly lower RPM at sea level.

[11] (Goldenberg, Conser, Joly, & Moroz, 2024)

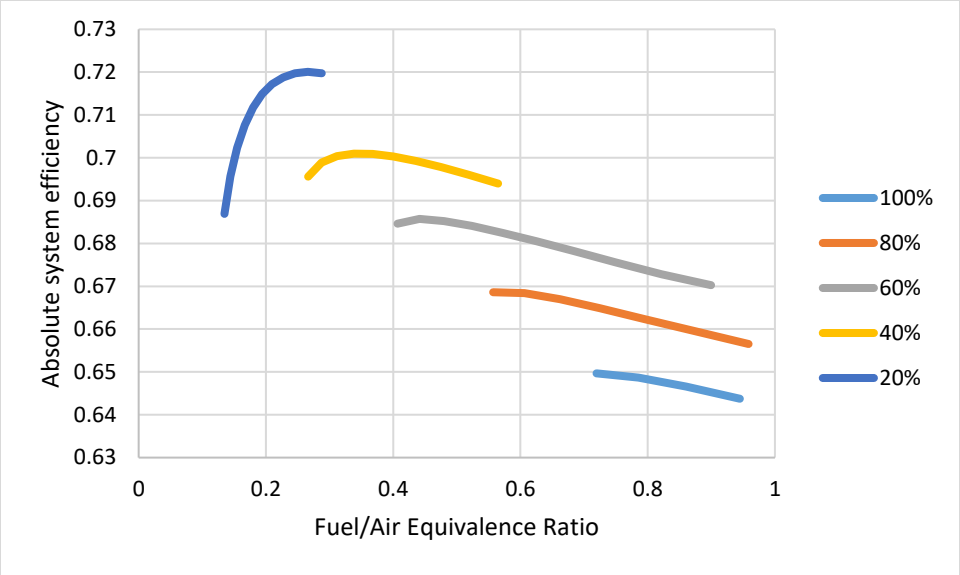

Figure 22: Absolute system efficiencies as a function of equivalence ratio at high altitude. Note that lower equivalence ratios correspond to higher turbocompressor speed.

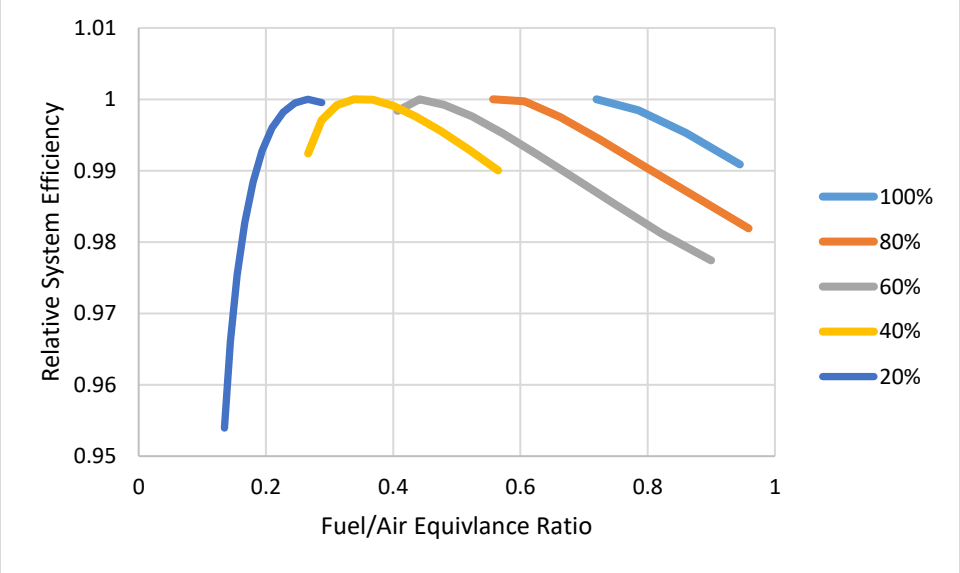

Figure 23: normalized system efficiencies at each load as a function of equivalence ratio at high altitude. Note that lower equivalence ratios correspond to higher turbocompressor speed.

One final post processing step and analysis is shown in Figure 22 and Figure 23, which has the same underlying data, but the former showing absolute values and the latter showing normalized curves for each load level. The information shows the system efficiency effect from the fuel/air equivalence ratio at variable load levels, both at high altitude conditions. The motivation for expressing the data by equivalence ratio is that it may be a more stable of a parameter and furthermore can be efficiently computed by a FADEC from direct flow measurements of the reactants. It must be noted that equivalence ratio close to unity indicates low air flow and

therefore lower RPM while lower equivalence ratio implies high RPM, airflow, and turbocompressor pressure ratio. What can be seen is that generally the relative efficiency is quite stable in the range of $0.2 < \phi < 0.8$, subject to the subsystem component limitations, which are the cause behind the limits of the curves. This suggests that a FADEC implementation may use equivalence ratio as a secondary closed loop feedback correction mechanism to maintaining optimal control, with feedforward setting initially chosen by a control table as graphically demonstrated in the previous figures.

CONCLUSIONS

We have demonstrated a multi-fidelity holistic approach to simulating an aero engine power system based on fuel cell electric drive. We presented a high efficiency implementation of such a system architecture, and developed fundamental design parameters of the fuel cell, turbomachinery, and thermal management system. We described in detail how AxSTREAM System Simulation platform was used to couple the various levels of fidelity of the subsystem models. We presented the system from the aspect of control and physicality and configuration that allows control and stability. Finally, we used the model to perform extensive multiparameter variation simulations over a range of boundary conditions that encompass the flight envelope and possible control inputs.

Analysis of the data generated by the simulations showed that the system is predicted to be highly performing across its intended operating envelope and controllable from a thermofluid and mechanical perspective. From the analysis, it was also suggested how a control scheme for maximizing performance of the system can be derived.

Finally, it is now emphasized that the holistic approach is what enabled the components of this system to be designed effectively. Only with a full system model that enables interaction of the interconnected components is it possible to evaluate and validate that the system design meets objectives. Such an approach is mandated by a systems engineering and model-based systems engineering (MBSE) paradigm. The tools utilized enabled the development of the model and execution on routine office computational equipment and within a timeframe that is conducive to fast design cycles, which further provides motivation to implement the holistic systems modeling approach when developing novel complex technologies.

CONTACT

The corresponding author is Vlad Goldenberg. He can be reached by email at vlad.goldenberg@softinway.com. SoftInWay can be reached by emailing info@softinway.com.

REFERENCES

Akmen, R. (2007). *Lectures and Objectives for the Course: Heat and Mass Transfer.* Kharkiv Polytechnic Institute.

Aungier, R. H. (2000). *Centrifugal Compressors.* New York: ASME.

Dixon, S. (2005). *Fluid Mechanics and Thermodynamics of Turbomachinery* (5th ed.). Elsevier.

Goldenberg, V., Conser, B., Joly, C., & Moroz, L. (2024). A HOLISTIC CONCEPTUAL SYNTHESIS AND ANALYSIS OF FUEL CELL SYSTEM ARCHITECTURES USING 1D COUPLED THERMOFLUID AND ELECTROCHEMICAL LUMPED PARAMETER SYSTEM SIMULATION. *Proceedings of ASME Turbo Expo 2024.* London, UK: ASME.

Incropera, F. P., Dewitt, D. P., Bergman, T. L., & Lavine, A. S. (2011). *Fundamentals of Heat and Mass Transfer.* United States of America: Wiley.

International Organization for Standardization. (1975). Standard Atmosphere. *ISO 2533:1975*.

Loftin, L. K. (1985). Mass-Flow Rate, Thrust, and Propulsive Efficiency. In L. K. Loftin, *Quest for performance: The evolution of modern aircraft. NASA SP-468* (p. Appendix E). National Aeronautics and Space Administration (NASA). Retrieved from https://www.hq.nasa.gov/pao/History/SP-468/app-e.htm

Orlov, M. (2013). *Theoretical Foundations of Heat Engineering. Heat and Mass Exchange.* Ulyanovsk: Ulyanovsk State Technical University.

Schuff, M. (2023). Towards Multi-Fidelity Simulations in the Context of the Virtual Engine. *Deutsche Gesellschaft für Luft-und Raumfahrt-Lilienthal-Oberth eV.* Stuttgart.

Sleicher, C., & Rouse, M. (1975). A Convenient Correlation for Heat Transfer to Constant and Variable Property Fluids in Turbulent Pipe Flow. *International Journal of Heat and Mass Transfer, 18*(5), 677-683.

Zaccaria, V., Stenfelt, M., Aslanidou, I., & Kyprianidis, K. G. (2018). Fleet monitoring and diagnostics framework based on digital twin of aero-engines. *Turbo expo: power for land, sea, and air* (p. V006T05A021). Oslo, Norway: American Society of Mechanical Engineers.